Active control of mixed convection in a rotating periodical two-pass duct by using trailing-wall transpiration

Jenn Jiang Hwang and Wei-Jyh Wang
Department of Mechanical Engineering, Chung-Hua University, Hsinchu, Taiwan, Republic of China

Received October 1999
Revised May 2000
Accepted May 2000

Keywords *Convection, Heat transfer, Flow*

Abstract *Deals with the flow reversal in a buoyancy-opposed rotating duct that causes heat transfer deterioration. An active technique of trailing-wall transpiration is adopted to check whether it can avoid the flow separation and subsequently improves the heat transfer deterioration. Finite-difference method is employed to solve the three-dimensional Navier-Stokes equations and the energy equation. Periodic conditions are used between the entrance and exit of a typical two-pass duct for the closure of the elliptic problem. The predicted results reveal that fluid withdrawal through the trailing wall can avoid the flow separation from the leading wall of the radial-outward duct (ROD) and thus eliminate local hot spots. In addition, the trailing-wall suction not only increases the peripherally averaged heat transfer but also reduces the friction loss in the ROD. In the radial-inward duct (RID), both the peripherally averaged heat transfer and peripherally averaged friction factor are augmented by trailing-wall injection and are degraded by the trailing-wall suction.*

Nomenclature

A_p = cross-sectional area at duct entrance
AR = area ratio of the total heat transfer surface of the module and the duct cross-section
A_T = total trailing surface area
De = duct hydraulic diameter [m]
f = friction factor
G = mass flow rate [kg s^{-1}]
Gr = rotational Grashof number, $\Omega^2 \cdot \beta_T \cdot q_w \cdot De^5/(\nu^2 \cdot k_f)$
k_f = air thermal conductivity [kW m^{-1} K–1]
Nu = local Nusselt number (see equation (13))
P,p = dimensionless and dimensional pressure
Pi = module pitch in z direction, i.e. $3De$ [m]
Pr = Prandtl number
Q = total heat input into the module [kW]
q_w = wall heat flux [kW m^{-2}]
Re = Reynolds number, $\overline{w}De/\nu$
Re_w = Wall Reynolds number, $\nu_w De/\nu$
Ri = Richardson number, Gr/Re^2
Ro = rotation number, $\Omega De/\overline{w}$
T = temperature [K]
T_b = local bulk mean temperature of air [K]
T_w = local wall temperature [K]
U,V,W = dimensionless local velocities in X, Y and Z directions, respectively
u,v,w = local velocities in X, Y and Z directions, respectively [m s^{-1}]
$\overline{w}$ = average flow velocity at the duct inlet [m s^{-1}]
X_o,x_o = dimensionless and dimensional radial distance from the rotation axis to the module
X,Y,Z = dimensionless rectangular coordinate (see Figure 1)
x,y,z = rectangular coordinate [m]

Support for this work was provided by the National Science Council of the Republic of China under contract No. NSC 85-2212-E-216-003.

Greek symbols

β = dimensionless pressure drop parameter
β_T = thermal expansion coefficient
η = dimensionless mass increase parameter, $\nu_w A_T/(3A_p\overline{w})$
γ = dimensionless air enthalpy rise parameter, $Q/(G \cdot c_p \cdot Pi)$
ϑ = dimensionless temperature, $(T - T_r)/(q_w \cdot De/k_f)$
ν = kinematic viscosity [$m^2\ s^{-1}$]
ρ = air density [kg m^{-3}]
Ω = angular rotation speed [s^{-1}]

Subscripts

b = bulk mean
f = fluid
L = leading wall
r = reference
s = smooth, stationary or static
w = wall

Superscripts

$\wedge$ = periodicity
$-$ = average
$*$ = with dimension

Introduction

Fluid flow and heat transfer in transpired-wall passages have received much attention in the past due to the wide applications and academic importance, such as porous electrodes of fuel cells, solar collectors, transpiration cooling of turbine blades, drying, boundary layer control, and many others. Among these, transpiration cooling of rotating blades is more related to the present study. In this method, most of the coolant from the blade base flows through internal passages and part of them transpires out through the porous skin to protect the blades from a high-temperature environment. In addition to the rotation-induced Coriolis and buoyancy forces, the wall injection/suction influences significantly the thermal behaviors within rotating passages. The ability to predict how wall transpiration affects the convective transport in rotating multiple-pass channels, even with a simple flow and wall geometry, is rather academically interesting and also valuable to the designer of aero-engines.

The influence of rotation on fluid flow and heat transfer in smooth or rib-roughened ducts has been studied extensively in the past three decades. Only some relevance works are reviewed below. In the experimental works, Johnston *et al.* (1972) investigated the effect of Coriolis force on the structure of turbulence in a rotating channel. It was found that the rotation number increases and diminishes turbulent mixing near the trailing and leading walls, respectively. Abdelmeguid and Spalding (1979) found that the buoyancy forces tend to reduce the laminar heat transfer rate but enhance the turbulent heat transfer rate in radially outward flow. Morris and Ayhan (1982) showed that the centrifugal buoyancy has an advantage effect on the heat transfer for the radially inward flow but an adverse effect for the radially outward flow. This kind of flow analogized to the mixed convection, buoyancy aiding and opposing, in a gravitational field. Morris and Ghavami-Nasr (1991) conducted heat transfer measurements in rotating rectangular channels and showed that the Coriolis-induced secondary flow enhances and degrades the local heat transfer over the trailing and leading walls, respectively. Han and Zhang (1992) studied the effect of uneven wall temperature on local heat transfer in a rotating square duct with radially outward flow. Results showed that the local transfer coefficients on the leading, trailing, and side-walls are altered by the uneven wall temperature. Morris and Rahmat-Abadi (1995) studied the effect of

internal ribs on the forced convection in rotating circular tubes. The effect of centrifugal buoyancy was also investigated and the combined effect of Coriolis forces and buoyancy was further demonstrated. As for the numerical simulation, Iacovides and Launder (1991) used the standard k-ε eddy-viscosity and algebraic second-moment closure turbulence models to predict the flow field and heat transfer in a rotating square duct. Results revealed that the flow instabilities lead the cross-flow from a two-vortex pattern to a four-vortex structure at higher rotating speeds. Medwell *et al.* (1991) employed a standard k-ε turbulence model together with the finite element method to predict heat transfer rates in a rotating cylindrical duct by considering the wall-conduction effect. Results showed that excluding the wall conduction effect the maximum wall temperature could be overestimated by about 50 percent. Tekriwal (1994) predicted heat transfer results with a standard k-ε model including buoyancy effects in the momentum equations. A reasonably qualitative agreement with experimental profiles of local Nusselt number was obtained, but the trailing side Nusselt number was still significantly underestimated. Dutta *et al.* (1996) employed the modeled turbulence generation terms for the Coriolis and buoyancy effects in the k-ε transport equations and obtained a better agreement with the experimental data.

All above-mentioned works, either numerical or experimental, are based on a single-pass flow passage. Recently, Wagner *et al.* (1991), Yang *et al.* (1992), and Hwang and Kuo (1997) carried out the experimental measurements on the convective heat transfer in radially rotating serpentine-shaped multiple-pass passages. Hwang and Lai (1998) and Hwang *et al.* (2000) performed numerical studies of the laminar convection in a radially rotating multiple-pass duct. General results in the rotating serpentine duct revealed that Coriolis force augments and degrades the heat transfer on high-pressure and low-pressure surfaces, respectively, while heat transfer benefits of the buoyancy depend on the directions of radial flow. The numerical predictions (Hwang and Lai, 1998; Hwang *et al.*, 2000) further revealed that the centrifugal buoyancy could cause the radial flows to reverse themselves near the leading wall of the radial-outward flow duct. A region of zero to low velocity is subsequently created near the leading wall that degrades the heat transfer considerably.

The purpose of this investigation is to extend the previous work (Hwang and Lai, 1998; Hwang *et al.*, 2000) to study numerically the effect of wall transpiration on the mixed convection in a rotating two-pass duct. Uniform fluid is transpired through the trailing wall of a rotating two-pass duct to check whether the active technique can control the flow reversal and eliminate the local hot spot in the rotating duct flow. The present numerical study is one of the first to study the effect of wall transpiration on the mixed convection in a radially rotating multiple-pass duct. Although the present prediction of laminar flow may not be of much appeal to the turbine-blade cooling, characterizing the flow control utilizing wall transpiration in buoyancy-opposing flow is still of academic interest.

Analysis

Problem physics

A schematic of the present problem is shown in Figure 1(a). The serpentine-duct geometry consists of an entrance duct and a number of identical two-pass modules. The flow is expected to attain, after an entrance section, a periodic flow regime in which the velocity fields repeat themselves from module to module. This study focuses on the periodic flows, i.e. the calculation of flow and heat transfer is limited to a typical two-pass module, without the need for the entrance region calculation. To resolve the periodic problem, the concepts and formulation previously used for periodic fully developed laminar flows in finned tubes (Patankar *et al.*, 1977) are employed, by which the flow and heat transfer characteristics are assumed to repeat themselves cyclically from the entrance of a two-pass channel to the next. It obviously not only provides considerable economy of computational effort but also ignores the relatively difficult task of solving the entrance-region problem. Figure 1(b) shows a typical periodic two-pass module, which consists of a radially inward duct, a radially outward duct, one 180° sharp turn, and two 90° meters. It rotates at a constant angular speed Ω about the axis in parallel with z direction. The duct of square cross-section is $20De$ in radial length, which is typical of the blade cooling passage. The distance from the axis of rotation to the test module is fixed at $x_o = 10De$. For simplicity, the radially inward duct and the radially outward duct are abbreviated as "RID" and "ROD", respectively, in the following discussion. With respect to the non-rotating flow, two additional forces act on the fluid particles in a radial plane due to the rotation, namely rotation-induced Coriolis force and centrifugal force. The Coriolis forces that drive the flow in the x and y directions are $2v \times \Omega$ and $-2u \times \Omega$, respectively.

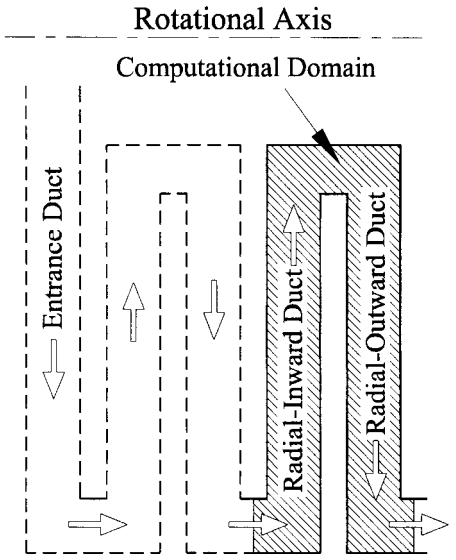

Figure 1a.
Computational domain in a serpentine duct

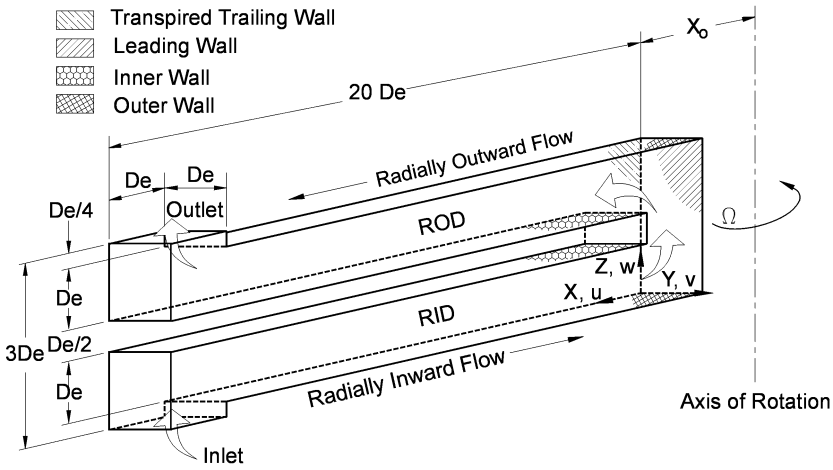

Figure 1b.
Configuration, dimensions, and the coordinate of the test module

The centrifugal inertia acting on the fluid particles in the x and y directions are $-\rho\Omega \times [\Omega \times (x + x_o)]$ and $-\rho\Omega \times (\Omega \times y)$, respectively. By using the Boussinesq approximation of a linear density-temperature relation, the centrifugal buoyancy can be further represented as $-\rho\beta_T(T - T_r)(x_o + x)\Omega^2$ and $-\rho\beta_T(T - T_r)y\Omega^2$, respectively. To facilitate the analysis, the flow is assumed to be steady and with constant properties, and the axial diffusion, viscous dissipation, and compression work are all ignored. Moreover, gravitational inertia is neglected due to its small magnitude compared to the rotational induced centrifugal force. On the trailing wall of the entire module, as shown in Figure 2, some fluid with a uniform velocity v_w is either injected into or sucked away from the duct.

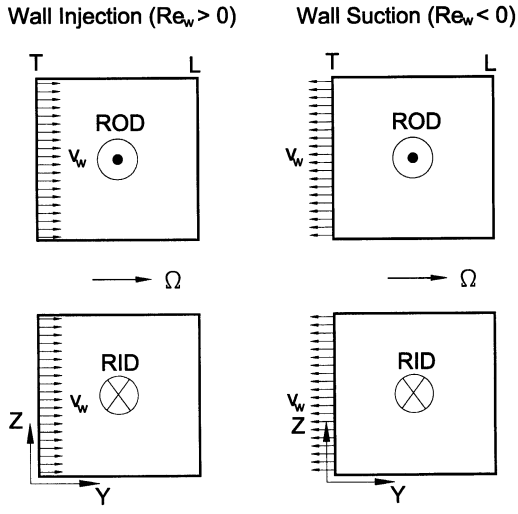

Figure 2.
Two kinds of trailing-wall boundary conditions investigated

The generalized fully developed regime

In the subsequent discussion, a general formulation according to the concepts of periodic fully developed flow and heat transfer is developed to accommodate the rotating periodical two-pass duct. Basically, the test section shown in Figure 1 can be regarded as a "periodically varied cross-section area" module in z direction; therefore, the physical quantities are decomposed in the z direction. According to Patankar *et al.* (1977), the pressure p and temperature T of a periodically fully developed flow can be decomposed as:

$$p(x,y,z) = -\beta^* z + \hat{p}\ (x,y,z) \tag{1}$$

$$T(x,y,z) = \gamma^* z + \hat{T}\ (x,y,z) \tag{2}$$

where both the global pressure drop parameter $\beta^* = [p(x,y,z) - p(x,y,z+Pi)]/Pi$ and the temperature increase parameter $\gamma^* = [T(x,y,z+Pi) - T(x,y,z)]/Pi$ are constants. The quantities of $\hat{p}$ and $\hat{T}$ identically repeat themselves from module to module. That is,

$$\hat{p}(x,y,z) = \hat{p}(x,y,z+Pi) = \hat{p}(x,y,z+2Pi) = \ldots \tag{3}$$

$$\hat{T}(x,y,z) = \hat{T}(x,y,z+Pi) = \hat{T}(x,y,z+2Pi) = \ldots \tag{4}$$

Since uniform flow is either injected into or sucked away from the radial duct through the trailing wall, the total mass flow rate across the duct should be either increased or decreased along the module width direction. The increment/decrease of the velocity magnitude w between the exit and entrance of each two-pass module should be identical, i.e.

$$w(x,y,z+Pi) - w(x,y,z) = w(x,y,z+2Pi) - w(x,y,z+Pi) = \ldots \tag{5}$$

Accordingly, a periodical velocity $\hat{w}$ and the velocity increment can be represented as

$$w(x,y,z) = \eta^* z + \hat{w}(x,y,z) \tag{6}$$

where η^* is a global mass increase parameter and is defined as

$$\eta^* = \frac{w(x,y,z+Pi - w(x,y,z)}{Pi} = \frac{\nu_w A_T}{Pi A_p} \tag{7}$$

where A_T and A_p are the total transpired-wall area of a two-pass module and the cross-sectional area at the duct entrance, respectively. Consequently, the equations governing the mass, momentum and energy can be written in dimensionless form as

$$\frac{\partial U}{\partial X}+\frac{\partial V}{\partial Y}+\frac{\partial \hat{W}}{\partial Z}+\eta=0 \tag{8}$$

$$U\frac{\partial U}{\partial X}+V\frac{\partial U}{\partial Y}+(\hat{W}+\eta Z)\frac{\partial U}{\partial Z}=-\frac{\partial \hat{P}}{\partial X}+\frac{1}{Re}\left(\frac{\partial^2 U}{\partial X^2}+\frac{\partial^2 U}{\partial Y^2}+\frac{\partial^2 U}{\partial Z^2}\right) + 2RoV - Ri\vartheta(X+X_o) \tag{9}$$

$$U\frac{\partial V}{\partial X}+V\frac{\partial V}{\partial Y}+(\hat{W}+\eta Z)\frac{\partial V}{\partial Z}=-\frac{\partial \hat{P}}{\partial Y}+\frac{1}{Re}\left(\frac{\partial^2 V}{\partial X^2}+\frac{\partial^2 V}{\partial Y^2}+\frac{\partial^2 V}{\partial Z^2}\right) - 2RoU - Ri\vartheta Y \tag{10}$$

$$U\frac{\partial \hat{W}}{\partial X}+V\frac{\partial \hat{W}}{\partial Y}+(\hat{W}+\eta Z)\frac{\partial(\hat{W}+\eta Z)}{\partial Z}=-\frac{\partial \hat{P}}{\partial Z}+\beta +\frac{1}{Re}\left(\frac{\partial^2 \hat{W}}{\partial X^2}+\frac{\partial^2 \hat{W}}{\partial Y^2}+\frac{\partial^2 W}{\partial Z^2}\right) \tag{11}$$

$$U\frac{\partial \vartheta}{\partial X}+V\frac{\partial \vartheta}{\partial Y}+(\hat{W}+\eta Z)\frac{\partial \vartheta}{\partial Z}=\frac{1}{RePr}\left(\frac{\partial^2 \vartheta}{\partial X^2}+\frac{\partial^2 \vartheta}{\partial Y^2}+\frac{\partial^2 \vartheta}{\partial Z^2}\right)-\gamma(\hat{W}+\eta Z) \tag{12}$$

where the dimensionless parameters are $X=x/De, Y=y/De, Z=z/De$, $U=u/\overline{w}, V=v/\overline{w}, W=w/\overline{w}, \vartheta=k_f(\hat{T}-T_r)/(q_w De), \hat{P}=\hat{p}/(\rho\overline{w}^2), \beta=\beta^* De/(\rho\overline{w}^2), \gamma=AR/(3Re\cdot Pr), \eta=\eta^* De/\overline{w}=41/3(Re_w/Re), Re=\overline{w}De/\nu, Ro=\Omega De/\overline{w}$, and $Ri=\Omega^2\beta_T q_w De^3/(k_f\overline{w}^2)$.

Boundary conditions

On the transpired trailing wall, uniform suction or injection is applied to the surfaces, i.e. $V=\pm\nu_w/\overline{w}$ (or Re_w/Re) and $U=W=0$, while no-slip conditions, i.e. $U=V=W=0$, are used for the remainder of the duct walls. In addition, each duct wall of the module is heated uniformly, i.e. $\partial\vartheta/\partial n=1$, where n denotes the outward dimensionless coordinate normal to the duct wall. At the module inlet and outlet, the periodicity is applied for the pressure, velocity and temperature components, i.e. $\Phi(X,Y,Z)=(\Phi(X,Y,Z+3)$, where Φ may be $\hat{P}, U, V$, and ϑ.

Solution procedure

The governing equations are numerically solved by the control-volume-based finite difference method (Patankar, 1980). The finite-difference procedure ensures conservation of mass, momentum, and energy over each control volume. Velocity control volumes are staggered with respect to the main

control volumes, and coupling of the pressure and velocity fields is treated via the SIMPLER (Van Doormaal and Raithby, 1992) pressure correction algorithm. In order to reduce numerical diffusion resulting from the existence of large cross-flow gradients and obliquity of the flow to the grid lines, the smooth hybrid central/skew upstream difference scheme (SCSUDS) is used for the diffusion and convective terms (Hwang *et al.*, 2000). The set of the differential equations over the entire region of interest is solved by obtaining new values for any desired variables, taking into account the latest known estimated values of the variable from the neighboring nodes. One iteration process is complete when, in the line-by-line technique, all lines in a direction have been accounted for. Because of the large variations in the source terms, under-relaxation is necessary for the dependent variables and the source terms to achieve convergence (Van Doormaal and Raithby, 1992). Line inversion iteration with typical under-relaxation values of 0.5 for the velocity terms and 0.7 for the pressure correction term are incorporated in the calculation. Solutions are considered to be converged at each test condition after two criteria are satisfied. First, the ratio of residual source (including mass and momentum) to the maximum flux across a control surface is required to be below 1.0×10^{-3}. Second, the iteration-to-iteration change is examined at every nodal location for all calculated values. However, to reduce the likelihood of false convergence related to small but persistent changes between successive iterations due to under-relaxation, examinations are implemented between iteration number I and I minus 20. The change in computed value, when compared to the maximum value in the domain, is required to be less than 5.0×10^{-6} for a solution to be considered converged. These comparison methods do not eliminate the possibility of false convergence, but it did reduce it. Typically, the former criterion is satisfied later.

All computations are performed on $72 \times 20 \times 50$ ($X \times Y \times Z$) straight-line grids in the present work. Additional runs for the coarser meshes, $50 \times 12 \times 30$, and the finer meshes, $90 \times 30 \times 70$, are taken for a check of grid independence. The parameters used to check the grid independence are axial velocity profile, pressure-drop parameter, and the local Nusselt number distribution. A comparison of the results of the two grid sizes, $72 \times 20 \times 50$ and $90 \times 30 \times 70$, shows that the maximum discrepancy in the axial velocity is 0.8 percent for the solid-wall condition ($Re_w = 0$). Moreover, computations for $Ro = 0.1, Re = 1{,}000$ and $Re_w = 3$ indicate a maximum change of 1.2 percent in local Nusselt number distribution between the solutions of $72 \times 20 \times 50$ and $90 \times 30 \times 70$ grids. These changes are so small that the accuracy of the solutions on the set of grid $72 \times 20 \times 50$ is deemed satisfactory.

Numerical computations of the periodical flows are difficult due to the fact that no boundary information is available in the main flow direction along which the discretization coefficients are large. Partly for this reason, the code takes as high as 5,000-9,000 iterations for convergence. On Convex-C3840, this is translated to between eight and 20 hours of CPU time.

Investigated parameters

After the velocity and temperature fields are obtained, the computations of the peripherally averaged Nusselt number are undertaken to evaluate the heat transfer performance in the rotating duct with a transpired trailing wall. Following the conventional definitions, the local span-averaged (Z) Nusselt number of the duct walls is defined as follows:

$$Nu_x = q_w \cdot De/[k_f \cdot (T_w - T_b)] = 1/(\vartheta_w - \vartheta_b). \tag{13}$$

Similarly, the peripherally averaged friction factor is calculated to assess the friction losses in the rotating multiple-pass duct

$$f\ Re = -2(\overline{\partial U/\partial n})_w. \tag{14}$$

Results and discussions

Flow structures

Figures 3-6 display the projection of secondary flow velocity vectors (arrows) and axial iso-speed contours (solid or dashed curves) at several axial stations (i.e. $X = 7.5$, 10 and 12.5) of the rotating two-pass duct under three different wall conditions, i.e. $Re_w = 0, -3$, and 3. The flow conditions are fixed at $Re = 1,000, Ro = 0.1$ and $Ri = 0.03$. All plots are viewed in the negative x direction. The solid curves correspond to the forward flow while the dashed curves correspond to the reversed flow.

In the solid-wall case ($Re_w = 0$), basically, the rotation-induced Coriolis and buoyancy forces affect the flow structures in the RID and ROD. The detailed description of their effects has been provided elsewhere (Iacovides and Launder, 1991) and only some important features are stressed here. As shown

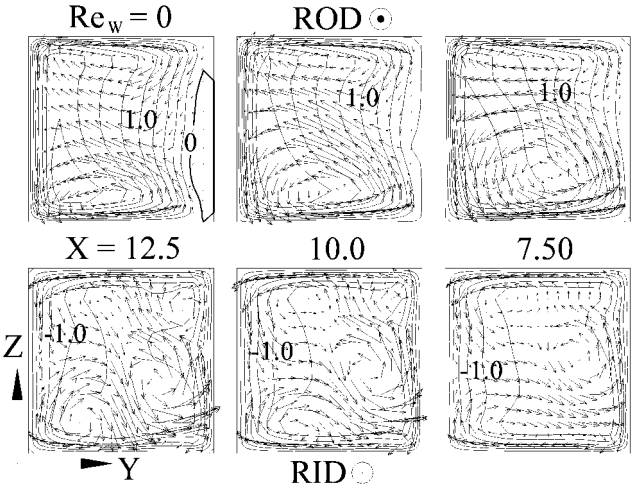

Figure 3.
Axial velocity and cross-flow structures at several axial stations for the solid wall ($Re_w = 3$) at $Ri = 0.03; Ro = 0.1$ and $Re = 1,000$

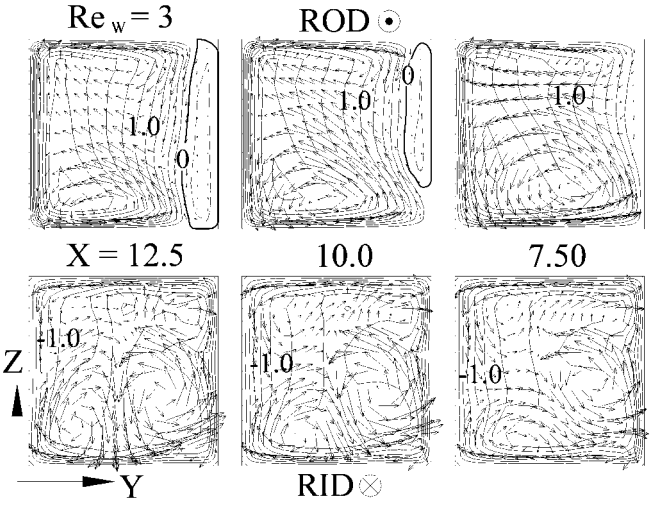

Figure 4.
Axial-velocity and crossflow structures at several axial stations for $Re_w = 3; Ri = 0.03;$ $Ro = 0.1$ and $Re = 1{,}000$

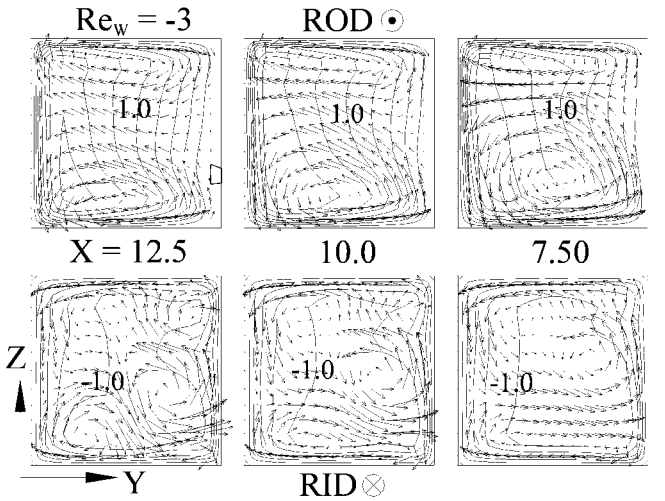

Figure 5.
Axial-velocity and crossflow structures at several axial stations for $Re_w = -3; Ri = 0.03;$ $Ro = 0.1$ and $Re = 1{,}000$

in Figure 3, the interaction of Coriolis force and centrifugal buoyancy significantly displaces the high-velocity core to the trailing wall in the ROD, but yields a relatively uniform axial iso-speed distribution in the RID. Notably, due to the opposed buoyancy in the ROD, the flow reversal occurs adjacent to the leading wall at $X = 12.5$. Meanwhile, an extremely small cross-flow intensity near the leading wall accompanies this flow reversal.

The effect of trailing-wall injection and suction on the secondary flow and axial-velocity distributions is shown in Figures 4 and 5, respectively. When the fluid is blown into the radial duct from the trailing wall ($Re_w = 3$ (Figure 4)), the flow-reversal phenomenon in the ROD seems to be severe. At $Re_w = 3$, the

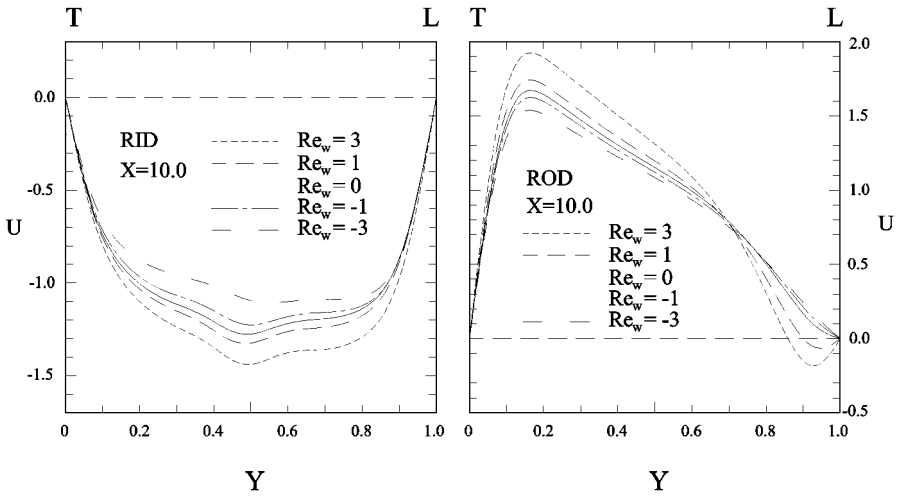

Figure 6.
effect of Re_w on the axial-velocity profile at $X = 10$

radial flow separates from the leading wall of the ROD at the location between $X = 7.5$ and 10. Contrarily, as the fluid is sucked away from the radial duct through the trailing wall with $Re_w = -3$ (Figure 5), the flow reversal at $X = 12.5$ of the ROD is hardly seen, indicating that the flow separation from the leading wall can be delayed by the wall-suction effect. As for the results in the RID, the wall transpiration does not alter the axial-velocity distribution too much. At the most, the maximum radial velocity in the core region is increased and decreased slightly with the wall injection and suction, respectively. As for the cross-flow structures, the trailing-wall injection (Figure 4) enhances and reduces the strength of cross-flow intensity in the RID and ROD, respectively. This fact may be explained as follows. When the fluid is injected into the radial duct through the trailing wall, the direction of wall velocity in the ROD is against the Coriolis force. The strength and size of the vortex pair induced by Coriolis force is therefore reduced. Contrarily, the wall injection in the RID is parallel to the Coriolis force, and thus enhances the cross-flow intensity. In contrast to the wall-injection results, the trailing-wall suction (Figure 5) enhances and reduces the cross-flow intensity in the ROD and RID, respectively.

Axial velocity and temperature profiles

Since the distributions of the thermal and fluid-flow fields are closely related to each other in the buoyancy-affected flow, the effect of wall Reynolds number on the axial-velocity and temperature profiles are simultaneously illustrated herein in Figures 6 and 7. In these Figures, the axial-velocity and temperature profiles are cut across the channel-centerlines ($Z = 0.5$, and 2.0) between the high- and low-pressure surfaces at $X = 10$. The letters L and T on this graph respectively denote the leading and trailing walls.

General tendency for the flow in rotating channels with solid walls (solid curves) is that the high-pressure surface corresponds to the fluid of high

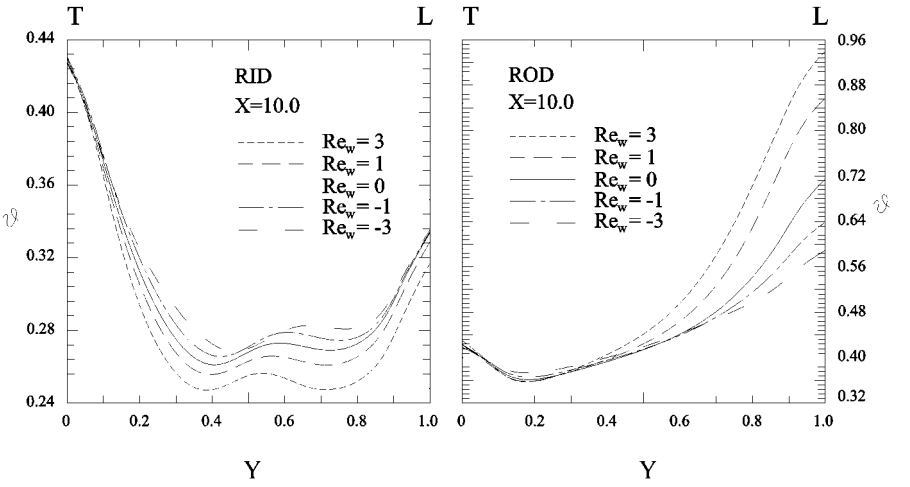

Figure 7.
Effect of Re_w on the temperature profile at $X = 10$

velocity/low temperature, and the low-pressure surface corresponds to the fluid of low velocity/high temperature (Iacovides and Launder, 1991). As for the wall transpiration effect in the RID, the magnitudes of axial velocity near both the trailing wall and the leading wall increase/decrease with wall injection/suction rate due to the flow accumulation (Figure 4). The flow temperatures therefore decrease with increasing/decreasing the wall injection/suction rate (Figure 7). In the ROD, however, the trailing-wall transpiration affects adversely the flow velocity near the trailing wall and leading wall. That is, the trailing-wall injection increases and decreases the axial velocity near the trailing wall and the leading wall, respectively. It is noteworthy that the decrease in flow velocity near the leading wall due to the trailing-wall injection results in a flow reversal. This fact may be explained as follows. As the fluid is injected into the radial duct through the trailing wall, the local mass flux of low-temperature/high-velocity fluids near the trailing wall is increased; this enlarges the local-buoyancy discrepancy between the trailing and leading walls of a radial plane. Such an imbalance of the local body force becomes significant as the flow moves downstream and, therefore, the trailing-wall fluids speed up downstream. For satisfying the mass conservation, the fluids near the leading wall should be retarded, come to rest and finally reverse themselves. The flow reversal causes a significant temperature rise near the leading wall (Figure 7) due to the accumulation of enthalpy upstream. Contrarily, trailing-wall suction reduces the local buoyancy discrepancy in the ROD, smooths the velocity profiles and subsequently prevents the flow separation from the leading wall; hence lower leading-wall temperatures (Figure 7).

Nusselt number and friction factor distributions

Figure 8 shows the effects of trailing-wall transpiration on the local Nusselt number distributions along the leading and trailing walls of the ROD and RID, respectively. The Reynolds number, rotation number and Richardson number

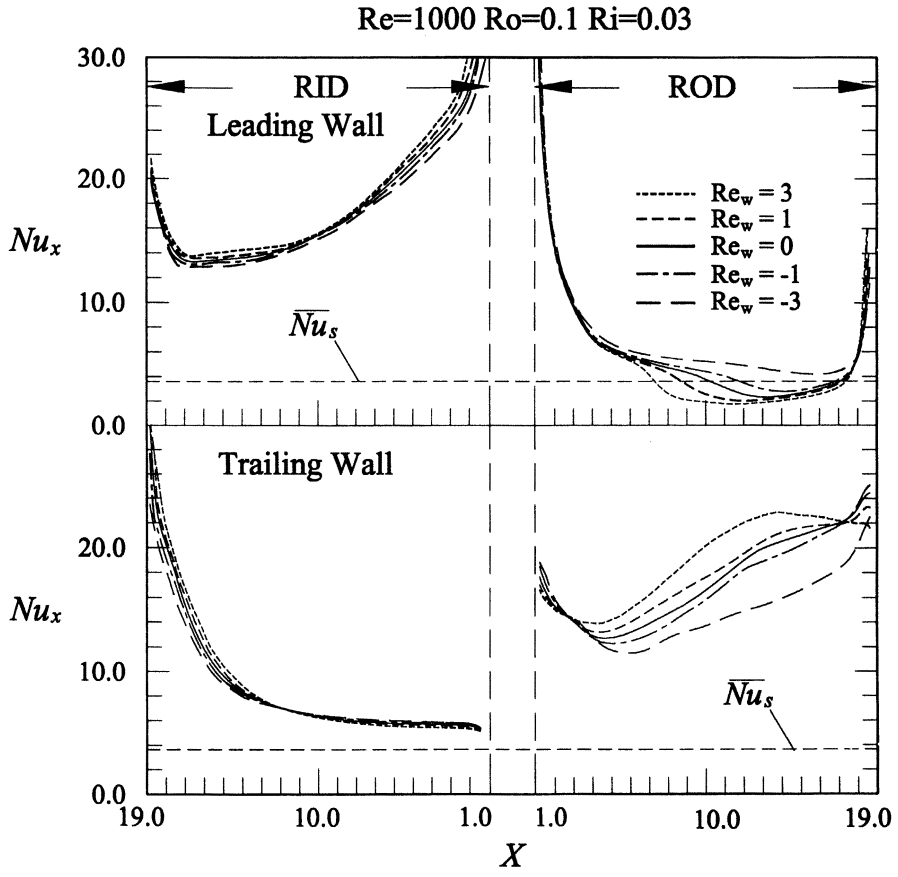

Figure 8.
Effect of Re_w on local Nusselt number distributions on the leading and trailing walls

are fixed at $Re = 1{,}000, Ro = 0.1$ and $Ri = 0.03$, respectively. The dashed straight line and the solid curve in each graph represent the value of fully developed stationary flows (i.e. $\overline{Nu}_s = 3.61$) and the solid-walled results ($Re_w = 0$), respectively. General trends of the solid-walled results show that, due to the Coriolis-force effect, the high-pressure surfaces have higher heat transfer coefficients than the low-pressure surfaces. In addition, a notable heat-transfer deterioration occurs on the leading wall of the ROD ($Nux < \overline{Nu}_s$) (Hwang and Lai, 1998).

In the ROD, obviously, the poor heat transfer on the leading wall has been improved gradually as the wall suction rate increases but has been degraded further by the wall injection. The local hot spots ($Nux < \overline{Nu}_s$) do not occur in the entire ROD for $Re_w = -3$. On the trailing wall, the heat transfer coefficient increases/decreases with increasing trailing-wall injection/suction rate. In the RID, the local Nusselt numbers on both the trailing and leading walls are increased/decreased with increasing injection/suction rate. This trend seems to be contrary to that of the boundary layer on the flat plate with wall suction and injection (Schlichting, 1979), in which suction thins the boundary layer and

greatly increases the heat transfer, while blowing thickens the boundary layer and decreases the heat transfer. It is not peculiar since, in the present work, the entire duct flow should be considered as a boundary layer, and an increase in the duct throughflow rate will increase the velocity gradient near the wall (Figures 4 and 6) and thus enhance the wall heat transfer. In addition, as mentioned above, the trailing-wall injection assists the Coriolis force in the RID to enhance the cross-flow intensity (Figure 3) and subsequently enhances the heat transfer.

Figure 9 shows the effect of trailing-wall transpiration on the axial variations of $f \cdot Re$, which is widely used to express the friction performance of straight ducts, along the leading and trailing walls of the ROD and the RID. The Reynolds number, rotation number and Richardson number are fixed at $Re = 1{,}000, Ro = 0.1$, and $Ri = 0.03$, respectively. The values on each wall are span-averaged. The horizontal dashed line on each graph represents the results of fully developed flows in straight stationary ducts, i.e. $f \cdot Re = 14.7$. In general, the wall Reynolds number dependence of the friction factor is largely similar to

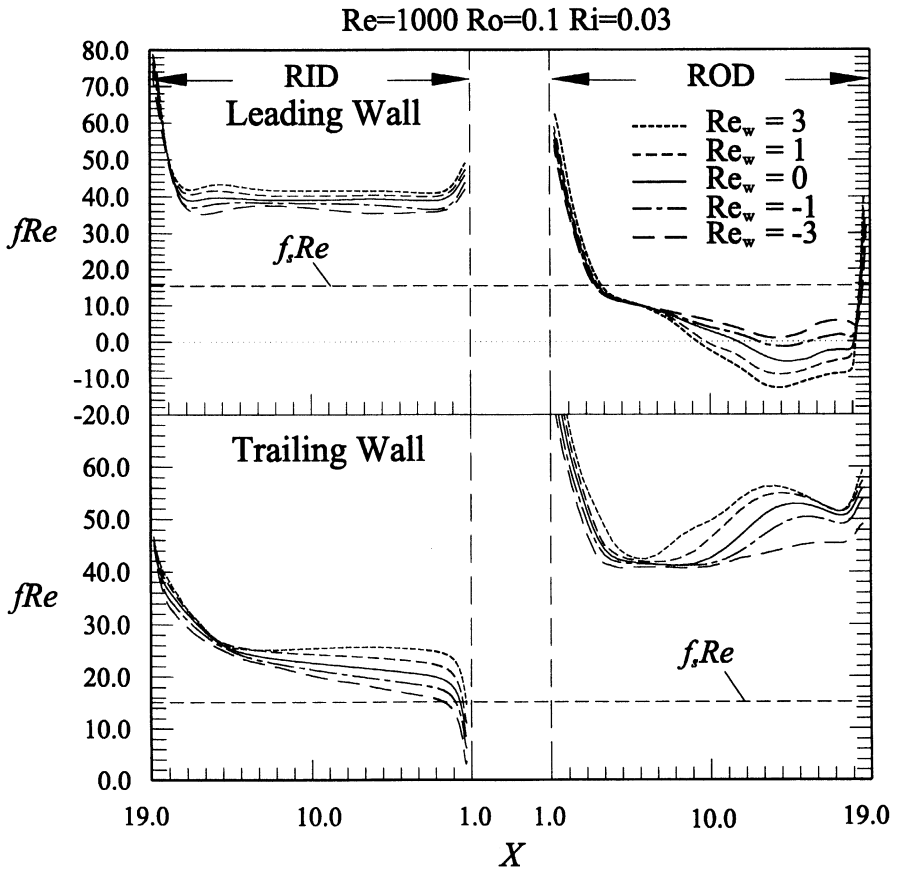

Figure 9.
Effect of Re_w on local friction factor distributions on the leading and trailing walls

that of the heat transfer coefficient (Figure 8). That is, in the RID the local friction factors on both the leading and trailing walls increase/decrease with increasing injection/suction rate. In the ROD, the values of $f \cdot Re$ on the leading wall decrease/increase with increasing the wall injection/suction rate, while the trend is reversed on the trailing wall. Note that the leading-wall friction factors are zero where flow separated from the duct wall (except for $Re_w = -3$). They subsequently become negative downstream because of the flow reversal.

Performance evaluation

Figure 10 shows the performance evaluation in the RID and ROD by considering the effect of the trailing-wall transpiration on the distributions of peripherally (four-wall) averaged heat transfer coefficient ($\overline{Nu}_x$) and friction factor. It is seen that the trailing-wall injection augments the peripherally averaged heat transfer in the RID, but meanwhile increases the friction factor. An opposite effect is found for the trailing-wall suction. In the ROD, the wall suction not only provides a higher peripherally averaged heat transfer

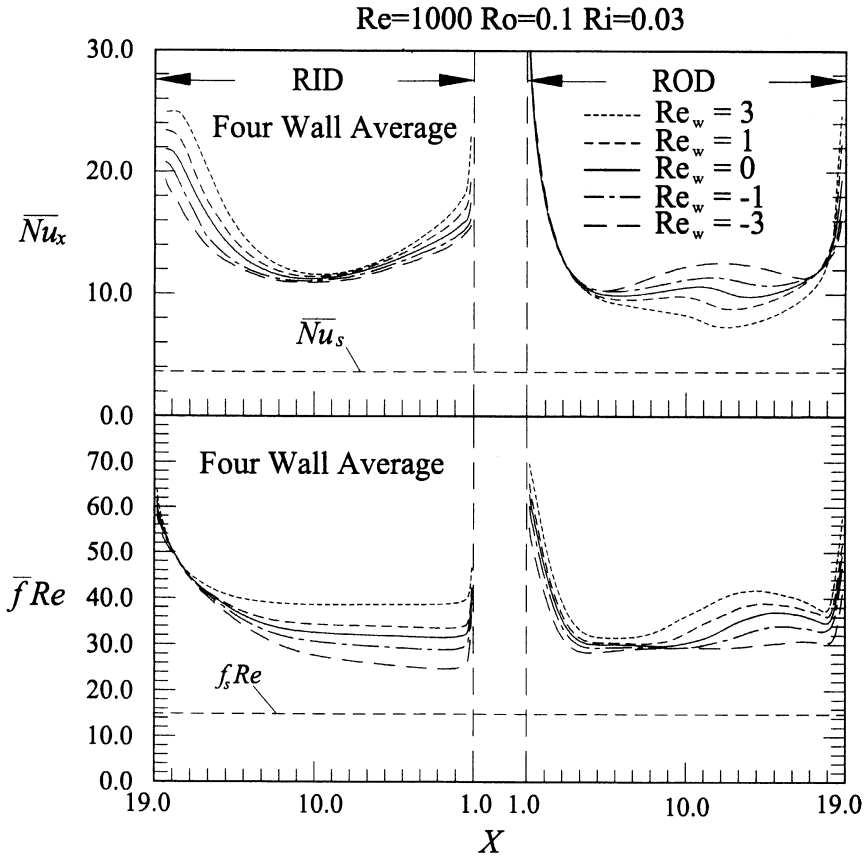

Figure 10.
Performance evaluations by comparing the peripherally averaged Nusselt number and friction factor distributions in the RID and ROD

coefficient but also yields a lower peripherally averaged friction factor than the solid wall. Contrarily, the wall suction reduces the heat transfer and increases the friction loss in the ROD.

Summary and conclusions

The effect of trailing-wall transpiration on the mixed convective phenomena in a radially rotating periodical two-pass duct has been studied numerically. The mechanisms of heat transfer augmentation or degradation due to the effects of wall injection and suction in the RID and ROD are discussed in detail and compared thereafter. Predictions reveal that fluid withdrawal through the trailing wall in the ROD is recommended, since it not only increases the peripherally averaged heat transfer but also reduces the friction loss in the ROD. Most importantly, it can retard and subsequently avoid the flow separation from the leading wall, and thus eliminate the heat transfer deterioration. In the RID, however, injection and suction on the trailing wall respectively augment and degrade the peripherally averaged heat transfer and friction factor.

No previous experimental works have considered the wall transpiration effect in rotating channel flows. Therefore, there are no data available with which the present results can be compared. However, the present results can serve as a theoretical basis for evaluating the significance of the wall injection or suction in rotating passages. A well-designed and carefully conducted experiment for the system considered here would be very appropriate.

References

Abdelmeguid, A.M. and Spalding, D.B. (1979), "Turbulent flow and heat transfer in pipes with buoyancy effect", *J. Fluid Mechanics*, Vol. 94, pp. 383-400.

Dutta, S., Anderson, M. and Han, J.C. (1996), "Prediction of turbulent heat transfer in rotating smooth square ducts", *Int. J. Heat Mass Transfer*, Vol. 39, pp. 2505-14.

Han, J.C. and Zhang, Y.M. (1992), "Effect of uneven wall temperature on local heat transfer in a rotating square channel with smooth walls of radial outward flow", *Trans. ASME, J. Heat Transfer*, Vol. 114, pp. 850-58.

Hwang, G.J. and Kuo, C.R. (1997), "Experimental studies and correlations of convective heat transfer in a radially rotating serpentine passage", *Trans. ASME, J. Heat Transfer*, Vol. 119, pp. 460-66.

Hwang, J.J. and Lai, D.Y. (1998), "Three-dimensional mixed convection in a rotating multiple-pass square channel", *Int. J. Heat Mass Transfer*, Vol. 41, pp. 979-91.

Hwang, J.J., Wang, W.J. and, Chen, C.K. (2000), "Buoyancy-driven flow reversal phenomena in radially rotating serpentine ducts", *Trans. ASME, J. Heat Transfer*, February.

Iacovides, H. and Launder, B.E. (1991), "Parametric and numerical study of fully developed flow and heat transfer in rotating rectangular ducts", *Trans. ASME, J. Turbomachinery*, Vol. 113, pp. 331-8.

Johnston, J.P., Halleen, R.M. and Lezius, D.K. (1972), "Effect of spanwise rotation on the structure of two-dimensional fully developed turbulent channel flow", *J. Fluid Mechanics*, Vol. 56, pp. 533-57.

Medwell, J.O., Morris, W.D., Xia, J.Y. and Taylor, C. (1991), "An investigation of convective heat transfer in a rotating coolant channel", *Trans. ASME, J. Turbomachinery*, Vol. 113, pp. 354-9.

Morris, W.D. and Ayhan, T. (1982), "An experimental study of turbulent heat transfer in a tube which rotates about an orthogonal axis", *Proc. XIV ICHMT Symposium on Heat and Mass Transfer in Rotating Machinery*, Dubrovnik.

Morris, W.D. and Ghavami-Nasr, G. (1991), "Heat transfer measurements in rectangular channels with orthogonal mode rotation", *Trans. ASME, J. Turbomachinery*, Vol. 113, pp. 339-45.

Morris, W.D. and Rahmat-Abadi, K.F. (1995), "Convective heat transfer in rotating ribbed tubes", *Int. J. Heat and Mass Transfer*, Vol. 39, pp. 2253-66.

Patankar, S.V. (1980), *Numerical Heat Transfer and Fluid Flow*, Hemisphere, Washington, DC.

Patankar, S.V., Liu, L.H. and Sparrow, E.M. (1977), "Fully developed flow and heat transfer ducts having periodic variations of the cross-sectional area", *Trans. ASME, J. Heat Transfer*, Vol. 99, pp. 180-86.

Schlichting, H. (1979), *Boundary Layer Theory*, McGraw-Hill, New York, NY.

Tekriwal, P. (1994), "Heat transfer predictions with extended k-ε turbulence model in radial cooling ducts rotating in orthogonal mode", *Trans. ASME, J. Heat Transfer*, Vol. 116, pp. 369-80.

Van Doormaal, J.P. and Raithby, G.D. (1992), "Enhancements of the simple method for predicting incompressible fluid flows", *Numerical Heat Transfer*, Part A, Vol. 7, pp. 147-63.

Wagner, J.H., Johnson, B.V. and Kopper, F.C. (1991), "Heat transfer in rotating serpentine passages with smooth walls", *Trans. ASME, J. Turbomachinery*, Vol. 113, pp. 321-30.

Yang, W.J., Zhang, N. and Chiou, J. (1992), "Local heat transfer in a rotating serpentine flow passage", *Trans. ASME, J. Heat Transfer*, Vol. 114, pp. 354-61.

Enter the Emerald Library

Access the MCB University Press online journal collection

Emerald News & Resources

Emerald news, service enhancements, marketing materials, librarian and end-user resources

Alert Service

Join our free alerting service and we'll email contents pages of the journals you select upon publication

Product Information

Detailed information on all Emerald products and services

Subscriber Registration

If you subscribe but have yet to register for online access, go to our subscriber registration page

Free Trials

Take advantage of our free 30 day trial of one or more journals

Help

Contact us with your technical and other customer service queries

---

Access | Home

MCB University Press

 60/62 Toller Lane Bradford England BD8 9BY
e-mail emer.tech.help@mcbup.co.uk